Study of χ_{cJ} radiative decays into a vector meson

M. Ablikim,[1] M. N. Achasov,[5] D. Alberto,[38] L. An,[9] Q. An,[36] Z. H. An,[1] J. Z. Bai,[1] R. Baldini,[17] Y. Ban,[23] J. Becker,[2] N. Berger,[1] M. Bertani,[17] J. M. Bian,[1] O. Bondarenko,[16] I. Boyko,[15] R. A. Briere,[3] V. Bytev,[15] X. Cai,[1] G. F. Cao,[1] X. X. Cao,[1] J. F. Chang,[1] G. Chelkov,[15,*] G. Chen,[1] H. S. Chen,[1] J. C. Chen,[1] M. L. Chen,[1] S. J. Chen,[21] Y. Chen,[1] Y. B. Chen,[1] H. P. Cheng,[11] Y. P. Chu,[1] D. Cronin-Hennessy,[35] H. L. Dai,[1] J. P. Dai,[1] D. Dedovich,[15] Z. Y. Deng,[1] I. Denysenko,[15,†] M. Destefanis,[38] Y. Ding,[19] L. Y. Dong,[1] M. Y. Dong,[1] S. X. Du,[42] R. R. Fan,[1] J. Fang,[1] S. S. Fang,[1] C. Q. Feng,[36] C. D. Fu,[1] J. L. Fu,[21] Y. Gao,[32] C. Geng,[36] K. Goetzen,[7] W. X. Gong,[1] M. Greco,[38] S. Grishin,[15] M. H. Gu,[1] Y. T. Gu,[9] Y. H. Guan,[6] A. Q. Guo,[22] L. B. Guo,[20] Y. P. Guo,[22] X. Q. Hao,[1] F. A. Harris,[34] K. L. He,[1] M. He,[1] Z. Y. He,[22] Y. K. Heng,[1] Z. L. Hou,[1] H. M. Hu,[1] J. F. Hu,[6] T. Hu,[1] B. Huang,[1] G. M. Huang,[12] J. S. Huang,[10] X. T. Huang,[25] Y. P. Huang,[1] T. Hussain,[37] C. S. Ji,[36] Q. Ji,[1] X. B. Ji,[1] X. L. Ji,[1] L. K. Jia,[1] L. L. Jiang,[1] X. S. Jiang,[1] J. B. Jiao,[25] Z. Jiao,[11] D. P. Jin,[1] S. Jin,[1] F. F. Jing,[32] N. Kalantar-Nayestanaki,[16] M. Kavatsyuk,[16] S. Komamiya,[31] W. Kuehn,[33] J. S. Lange,[33] J. K. C. Leung,[30] Cheng Li,[36] Cui Li,[36] D. M. Li,[42] F. Li,[1] G. Li,[1] H. B. Li,[1] J. C. Li,[1] Lei Li,[1] N. B. Li,[20] Q. J. Li,[1] W. D. Li,[1] W. G. Li,[1] X. L. Li,[25] X. N. Li,[1] X. Q. Li,[22] X. R. Li,[1] Z. B. Li,[28] H. Liang,[36] Y. F. Liang,[27] Y. T. Liang,[33] G. R. Liao,[8] X. T. Liao,[1] B. J. Liu,[30] B. J. Liu,[29] C. L. Liu,[3] C. X. Liu,[1] C. Y. Liu,[1] F. H. Liu,[26] Fang Liu,[1] Feng Liu,[12] G. C. Liu,[1] H. Liu,[1] H. B. Liu,[6] H. M. Liu,[1] H. W. Liu,[1] J. P. Liu,[40] K. Liu,[23] K. Liu,[6] K. Y. Liu,[19] Q. Liu,[34] S. B. Liu,[36] X. Liu,[18] X. H. Liu,[1] Y. B. Liu,[22] Y. W. Liu,[36] Yong Liu,[1] Z. A. Liu,[1] Z. Q. Liu,[1] H. Loehner,[16] G. R. Lu,[10] H. J. Lu,[11] J. G. Lu,[1] Q. W. Lu,[26] X. R. Lu,[6] Y. P. Lu,[1] C. L. Luo,[20] M. X. Luo,[41] T. Luo,[1] X. L. Luo,[1] C. L. Ma,[6] F. C. Ma,[19] H. L. Ma,[1] Q. M. Ma,[1] T. Ma,[1] X. Ma,[1] X. Y. Ma,[1] M. Maggiora,[38] Q. A. Malik,[37] H. Mao,[1] Y. J. Mao,[23] Z. P. Mao,[1] J. G. Messchendorp,[16] J. Min,[1] R. E. Mitchell,[14] X. H. Mo,[1] N. Yu. Muchnoi,[5] Y. Nefedov,[15] Z. Ning,[1] S. L. Olsen,[24] Q. Ouyang,[1] S. Pacetti,[17] M. Pelizaeus,[34] K. Peters,[7] J. L. Ping,[20] R. G. Ping,[1] R. Poling,[35] C. S. J. Pun,[30] M. Qi,[21] S. Qian,[1] C. F. Qiao,[6] X. S. Qin,[1] J. F. Qiu,[1] K. H. Rashid,[37] G. Rong,[1] X. D. Ruan,[9] A. Sarantsev,[15,‡] J. Schulze,[2] M. Shao,[36] C. P. Shen,[34] X. Y. Shen,[1] H. Y. Sheng,[1] M. R. Shepherd,[1] X. Y. Song,[1] S. Sonoda,[31] S. Spataro,[38] B. Spruck,[33] D. H. Sun,[1] G. X. Sun,[1] J. F. Sun,[1] S. S. Sun,[1] X. D. Sun,[1] Y. J. Sun,[36] Y. Z. Sun,[1] Z. J. Sun,[1] Z. T. Sun,[36] C. J. Tang,[27] X. Tang,[1] X. F. Tang,[8] H. L. Tian,[1] D. Toth,[35] G. S. Varner,[34] X. Wan,[1] B. Q. Wang,[23] K. Wang,[1] L. L. Wang,[4] L. S. Wang,[1] M. Wang,[25] P. Wang,[1] P. L. Wang,[1] Q. Wang,[1] S. G. Wang,[23] X. L. Wang,[36] Y. D. Wang,[36] Y. F. Wang,[1] Y. Q. Wang,[25] Z. Wang,[1] Z. G. Wang,[1] Z. Y. Wang,[1] D. H. Wei,[8] Q. G. Wen,[36] S. P. Wen,[1] U. Wiedner,[2] L. H. Wu,[1] N. Wu,[1] W. Wu,[19] Z. Wu,[1] Z. J. Xiao,[20] Y. G. Xie,[1] G. F. Xu,[1] G. M. Xu,[23] H. Xu,[1] Y. Xu,[22] Z. R. Xu,[36] Z. Z. Xu,[36] Z. Xue,[1] L. Yan,[36] W. B. Yan,[36] Y. H. Yan,[13] H. X. Yang,[1] M. Yang,[1] T. Yang,[9] Y. Yang,[20] Y. X. Yang,[8] M. Ye,[1] M. H. Ye,[4] B. X. Yu,[1] C. X. Yu,[22] L. Yu,[12] C. Z. Yuan,[1] W. L. Yuan,[20] Y. Yuan,[1] A. A. Zafar,[37] A. Zallo,[17] Y. Zeng,[13] B. X. Zhang,[1] B. Y. Zhang,[1] C. C. Zhang,[1] D. H. Zhang,[1] H. H. Zhang,[28] H. Y. Zhang,[1] J. Zhang,[20] J. W. Zhang,[1] J. Y. Zhang,[1] J. Z. Zhang,[1] L. Zhang,[21] S. H. Zhang,[1] T. R. Zhang,[20] X. J. Zhang,[1] X. Y. Zhang,[25] Y. Zhang,[1] Y. H. Zhang,[1] Z. P. Zhang,[36] Z. Y. Zhang,[40] G. Zhao,[1] H. S. Zhao,[1] Jiawei Zhao,[36] Jingwei Zhao,[1] Lei Zhao,[36] Ling Zhao,[1] M. G. Zhao,[22] Q. Zhao,[1] S. J. Zhao,[42] T. C. Zhao,[39] X. H. Zhao,[21] Y. B. Zhao,[1] Z. G. Zhao,[36] Z. L. Zhao,[9] A. Zhemchugov,[15,*] B. Zheng,[1] J. P. Zheng,[1] Y. H. Zheng,[6] Z. P. Zheng,[1] B. Zhong,[1] J. Zhong,[2] L. Zhong,[32] L. Zhou,[1] X. K. Zhou,[6] X. R. Zhou,[36] C. Zhu,[1] K. Zhu,[1] K. J. Zhu,[1] S. H. Zhu,[1] X. L. Zhu,[32] X. W. Zhu,[1] Y. S. Zhu,[1] Z. A. Zhu,[1] J. Zhuang,[1] B. S. Zou,[1] J. H. Zou,[1] J. X. Zuo,[1] and P. Zweber[35]

(BESIII Collaboration)

[1]*Institute of High Energy Physics, Beijing 100049, Peoples Republic of China*
[2]*Bochum Ruhr-University, 44780 Bochum, Germany*
[3]*Carnegie Mellon University, Pittsburgh, Pennsylvania 15213, USA*
[4]*China Center of Advanced Science and Technology, Beijing 100190, Peoples Republic of China*
[5]*G. I. Budker Institute of Nuclear Physics SB RAS (BINP), Novosibirsk 630090, Russia*
[6]*Graduate University of Chinese Academy of Sciences, Beijing 100049, Peoples Republic of China*
[7]*GSI Helmholtzcentre for Heavy Ion Research GmbH, D-64291 Darmstadt, Germany*
[8]*Guangxi Normal University, Guilin 541004, Peoples Republic of China*
[9]*Guangxi University, Naning 530004, Peoples Republic of China*
[10]*Henan Normal University, Xinxiang 453007, Peoples Republic of China*
[11]*Huangshan College, Huangshan 245000, Peoples Republic of China*
[12]*Huazhong Normal University, Wuhan 430079, Peoples Republic of China*
[13]*Hunan University, Changsha 410082, Peoples Republic of China*
[14]*Indiana University, Bloomington, Indiana 47405, USA*
[15]*Joint Institute for Nuclear Research, 141980 Dubna, Russia*

[16]*KVI/University of Groningen, 9747 AA Groningen, The Netherlands*
[17]*Laboratori Nazionali di Frascati—INFN, 00044 Frascati, Italy*
[18]*Lanzhou University, Lanzhou 730000, Peoples Republic of China*
[19]*Liaoning University, Shenyang 110036, Peoples Republic of China*
[20]*Nanjing Normal University, Nanjing 210046, Peoples Republic of China*
[21]*Nanjing University, Nanjing 210093, Peoples Republic of China*
[22]*Nankai University, Tianjin 300071, Peoples Republic of China*
[23]*Peking University, Beijing 100871, Peoples Republic of China*
[24]*Seoul National University, Seoul, 151-747 Korea*
[25]*Shandong University, Jinan 250100, Peoples Republic of China*
[26]*Shanxi University, Taiyuan 030006, Peoples Republic of China*
[27]*Sichuan University, Chengdu 610064, Peoples Republic of China*
[28]*Sun Yat-Sen University, Guangzhou 510275, Peoples Republic of China*
[29]*The Chinese University of Hong Kong, Shatin, N. T., Hong Kong*
[30]*The University of Hong Kong, Pokfulam, Hong Kong*
[31]*The University of Tokyo, Tokyo 113-0033 Japan*
[32]*Tsinghua University, Beijing 100084, Peoples Republic of China*
[33]*Universitaet Giessen, 35392 Giessen, Germany*
[34]*University of Hawaii, Honolulu, Hawaii 96822, USA*
[35]*University of Minnesota, Minneapolis, Minnesota 55455, USA*
[36]*University of Science and Technology of China, Hefei 230026, Peoples Republic of China*
[37]*University of the Punjab, Lahore-54590, Pakistan*
[38]*University of Turin and INFN, Turin, Italy*
[39]*University of Washington, Seattle, Washington 98195, USA*
[40]*Wuhan University, Wuhan 430072, Peoples Republic of China*
[41]*Zhejiang University, Hangzhou 310027, Peoples Republic of China*
[42]*Zhengzhou University, Zhengzhou 450001, Peoples Republic of China*

(Received 29 March 2011; published 10 June 2011)

The decays $\chi_{cJ} \to \gamma V$ ($V = \phi$, ρ^0, ω) are studied with a sample of radiative $\psi' \to \gamma\chi_{cJ}$ events in a sample of $(1.06 \pm 0.04) \times 10^8 \psi'$ events collected with the BESIII detector. The branching fractions are determined to be: $\mathcal{B}(\chi_{c1} \to \gamma\phi) = (25.8 \pm 5.2 \pm 2.3) \times 10^{-6}$, $\mathcal{B}(\chi_{c1} \to \gamma\rho^0) = (228 \pm 13 \pm 22) \times 10^{-6}$, and $\mathcal{B}(\chi_{c1} \to \gamma\omega) = (69.7 \pm 7.2 \pm 6.6) \times 10^{-6}$. The decay $\chi_{c1} \to \gamma\phi$ is observed for the first time. Upper limits at the 90% confidence level on the branching fractions for χ_{c0} and χ_{c2} decays into these final states are determined. In addition, the fractions of the transverse polarization component of the vector meson in $\chi_{c1} \to \gamma V$ decays are measured to be $0.29^{+0.13+0.10}_{-0.12-0.09}$ for $\chi_{c1} \to \gamma\phi$, $0.158 \pm 0.034^{+0.015}_{-0.014}$ for $\chi_{c1} \to \gamma\rho^0$, and $0.247^{+0.090+0.044}_{-0.087-0.026}$ for $\chi_{c1} \to \gamma\omega$, respectively. The first errors are statistical and the second ones are systematic.

DOI: 10.1103/PhysRevD.83.112005 PACS numbers: 13.20.Gd, 14.40.Lb

I. INTRODUCTION

Doubly radiative decays of the type $\psi \to \gamma X \to \gamma\gamma V$, where V is either a ϕ, ρ^0, or ω meson, provide information on the flavor content of the C-even resonance X and on the gluon hadronization dynamics in the process [1–3]. The spin and charge dependent couplings in radiative decays reveal detailed information which is particularly useful in the search for glueball and hybrid states [4]. For the case where $X = \chi_{cJ}$, the decay of the P-wave χ_{cJ} to γV may provide an independent window for understanding possible glueball dynamics and validating theoretical techniques [5].

Table I shows the theoretical predictions for χ_{cJ} radiative decays to a vector meson from perturbative quantum chromodynamics (pQCD) [2], nonrelativistic QCD (NRQCD) [3], and NRQCD plus QED contributions (NRQCD + QED) [3], and recent results from the CLEO experiment [6]. The experimental results for $\mathcal{B}(\chi_{c1} \to \gamma\rho^0, \gamma\omega)$ are an order of magnitude higher than the corresponding theoretical predictions. However, by including nonperturbative QCD hadronic loop contributions, a recent pQCD calculation [7] obtains results in agreement with the CLEO measurements. Improved measurements of χ_{cJ} radiative decays to vector mesons using the large BESIII ψ' sample will provide tighter constraints on theoretical calculations.

In this paper, we present measurements of radiative decays of the χ_{cJ} to the light vector mesons. The measurements have improved precision compared to CLEO's

[*]also at the Moscow Institute of Physics and Technology, Moscow, Russia
[†]on leave from the Bogolyubov Institute for Theoretical Physics, Kiev, Ukraine
[‡]also at the PNPI, Gatchina, Russia

TABLE I. Comparison of theoretical predictions on the branching fractions for χ_{cJ} radiative decays to a vector meson (in units of 10^{-6}) and measurements from the CLEO experiment. The upper limits are at the 90% confidence level (C.L.).

Mode	CLEO [6]	pQCD [2]	NRQCD [3]	NRQCD + QED [3]
$\chi_{c0} \to \gamma\rho^0$	<9.6	1.2	3.2	2.0
$\chi_{c1} \to \gamma\rho^0$	$243 \pm 19 \pm 22$	14	41	42
$\chi_{c2} \to \gamma\rho^0$	<50	4.4	13	38
$\chi_{c0} \to \gamma\omega$	<8.8	0.13	0.35	0.22
$\chi_{c1} \to \gamma\omega$	$83 \pm 15 \pm 12$	1.6	4.6	4.7
$\chi_{c2} \to \gamma\omega$	<7.0	0.5	1.5	4.2
$\chi_{c0} \to \gamma\phi$	<6.4	0.46	1.3	0.03
$\chi_{c1} \to \gamma\phi$	<26	3.6	11	11
$\chi_{c2} \to \gamma\phi$	<13	1.1	3.3	6.5

results, and $\chi_{c1} \to \gamma\phi$ decay is observed for the first time. In addition, the fraction of the transverse polarization component of the vector meson in $\chi_{c1} \to \gamma V$ decay is studied, and the results indicate that the longitudinal component for $\chi_{c1} \to \gamma V$ decay is dominant. This observation may help in the theoretical understanding of $\chi_{c1} \to \gamma V$ decays.

II. BEPCII COLLIDER AND BESIII DETECTOR

BEPCII/BESIII [8] is a major upgrade of the BESII experiment at the BEPC accelerator [9] for studies of hadron spectroscopy and τ-charm physics [10]. The design peak luminosity of the double-ring e^+e^- collider, BEPCII, is 10^{33} cm^{-2} s^{-1} at a beam current of 0.93 A. The BESIII detector with a geometrical acceptance of 93% of 4π, consists of the following main components: (1) a small-celled, helium-based main draft chamber (MDC) with 43 layers. The average single wire resolution is 135 μm, and the momentum resolution for 1 GeV/c charged particles in a 1 T magnetic field is 0.5%; (2) an electromagnetic calorimeter (EMC) made of 6240 CsI (Tl) crystals arranged in a cylindrical shape (barrel) plus two end-caps. For 1.0 GeV photons, the energy resolution is 2.5% in the barrel and 5% in the end-caps, and the position resolution is 6 mm in the barrel and 9 mm in the end-caps; (3) a time-of-flight system (TOF) for particle identification composed of a barrel part made of two layers with 88 pieces of 5 cm thick, 2.4 m long plastic scintillators in each layer, and two end-caps with 96 fan-shaped, 5 cm thick, plastic scintillators in each end-cap. The time resolution is 80 ps in the barrel, and 110 ps in the end-caps, corresponding to a 2σ K/π separation for momenta up to about 1.0 GeV/c; (4) a muon chamber system made of 1000 m^2 of resistive plate chambers arranged in 9 layers in the barrel and 8 layers in the end-caps and incorporated in the return iron of the superconducting magnet. The position resolution is about 2 cm.

The optimization of the event selection and the estimation of physics backgrounds are performed through Monte Carlo simulations. The GEANT4-based simulation software BOOST [11] includes the geometric and material description of the BESIII detectors, the detector response and digitization models, as well as the tracking of the detector running conditions and performance. The production of the ψ' resonance is simulated by the Monte Carlo event generator KKMC [12], while the decays are generated by EVTGEN [13] for known decay modes with branching ratios being set to the PDG [14] world average values, and by LUNDCHARM [15] for the remaining unknown decays. The analysis is performed in the framework of the BESIII offline software system [16] which takes care of the detector calibration, event reconstruction and data storage.

III. DATA ANALYSIS

A data sample of $(1.06 \pm 0.04) \times 10^8$ ψ' events collected with the BESIII detector is used in this analysis, and an independent sample of about 42.6 pb^{-1} taken at $\sqrt{s} = 3.65$ GeV is utilized to determine the potential background contribution from the continuum. In this paper, we focus on the exclusive decays of $\psi' \to \gamma_l\chi_{cJ}$, $\chi_{cJ} \to \gamma_h V$, where $\gamma_l(\gamma_h)$ designates the lower (higher) energy photon and V is either a ϕ, ρ^0, or ω meson. The ϕ, ρ^0, and ω candidates are reconstructed in the K^+K^-, $\pi^+\pi^-$, and $\pi^+\pi^-\pi^0$ decay modes, respectively.

Charged tracks are reconstructed in the MDC, and the number of charged tracks is required to be two with net charge zero. For each track, the polar angle must satisfy $|\cos\theta| < 0.93$, and it must be within ± 10 cm of the interaction point in the beam direction and within ± 1 cm of the beam line in the plane perpendicular to the beam. Since the efficiency of particle identification (PID) is lower for higher momentum (> 1 GeV/c) charged tracks, only the lower momentum charged track is required to be identified as a K or π.

Electromagnetic showers are reconstructed by clustering EMC crystal energies. The energy deposited in nearby TOF counters is included to improve the reconstruction

efficiency and energy resolution. Showers identified as photon candidates must satisfy fiducial and shower-quality requirements. The photon candidate showers reconstructed from the barrel region ($|\cos\theta| < 0.8$) must have a minimum energy of 25 MeV, while those in the end-caps ($0.86 < |\cos\theta| < 0.92$) must have at least 50 MeV. The showers in the angular range between the barrel and end-cap are poorly reconstructed and excluded from the analysis. To eliminate showers from charged particles, a photon must be separated by at least 10° from any charged track. EMC cluster timing requirements are used to suppress electronic noise and energy deposits unrelated to the event.

In order to choose the correct combination and improve the mass resolution, a four-constraint kinematic fit (4C-fit) is done under the assumption of energy-momentum conservation. Candidates with $\chi^2 \leq 100$ for this fit are retained. If an event has more than one candidate, the candidate with the smallest χ^2 is kept.

For $\psi' \to \gamma\gamma\omega$ ($\omega \to \pi^+\pi^-\pi^0$) candidates, the gammas from the π^0 decay are selected as those that give the minimum of

$$\sqrt{\left(\frac{M_{\gamma_1\gamma_2} - M_{\pi^0}}{\sigma_{\pi^0}}\right)^2 + \left(\frac{M_{\pi^+\pi^-\gamma_1\gamma_2} - M_{\omega}}{\sigma_{\omega}}\right)^2},$$

where $M_{\gamma_1\gamma_2}$ is the invariant mass of the photon pair, M_{π^0} (M_ω) is the nominal mass of π^0 (ω), σ_{π^0} (σ_ω) is the mass resolution determined from MC simulation and is about 7 MeV/c^2 (6 MeV/c^2). A π^0 mass constraint for the $\gamma\gamma\omega$ channel is included by doing a five-constraint kinematic fit (5C-fit), and events with $\chi^2_{5C} \leq 100$ are kept as $\psi' \to \gamma_l\gamma_h\omega$ ($\omega \to \pi^+\pi^-\pi^0$) candidates.

To suppress background from multiphoton hadronic decays of the ψ', $|M_{\gamma_l\gamma_h} - M_\eta| \geq 25$ MeV/c^2 for $\gamma\gamma\phi$, $M_{\gamma_l\gamma_h} \geq 600$ MeV/c^2 for $\gamma\gamma\rho^0$, and $|M_{\gamma_l\gamma_h} - M_\eta| \geq 25$ MeV/c^2 and $|M_{\gamma_l\gamma_h} - M_{\pi^0}| \geq 15$ MeV/c^2 for $\gamma\gamma\omega$ are required. Here M_{π^0} and M_η are the nominal masses of π^0 and η, respectively. The background from $\psi' \to \gamma_h\eta'$, $\eta' \to \gamma_l V$ ($V = \rho^0, \omega$) is suppressed by requiring $|M_{\gamma_l V} - M_{\eta'}| > 15$ MeV/c^2.

In $\chi_{cJ} \to \gamma\rho^0$, there are potential backgrounds from QED $e^+e^- \to \gamma e^+e^-$ and $\mu^+\mu^-$ events where the leptons are misidentified as pions. To reject electrons, the ratio of the energy deposited in the EMC to the momentum measured in the MDC ($E_{\rm EMC}/cp_{\rm MDC}$) of tracks must be less than 0.8. To reject muons, tracks are removed if the number of layers with hits in the muon chamber is greater than three. The QCD backgrounds remaining can be effectively eliminated by requiring the opening angle between the two pions, $\cos\theta_{\pi^+\pi^-}$, satisfy $\cos\theta_{\pi^+\pi^-} > -0.8$, and that between the two photons, $\cos\theta_{\gamma_l\gamma_h}$, satisfy $-0.98 < \cos\theta_{\gamma_l\gamma_h} < 0.5$, in the laboratory frame.

Figure 1 shows the K^+K^-, $\pi^+\pi^-$, and $\pi^+\pi^-\pi^0$ invariant mass distributions for the candidate events. The curves show the best fit to the mass spectra using a

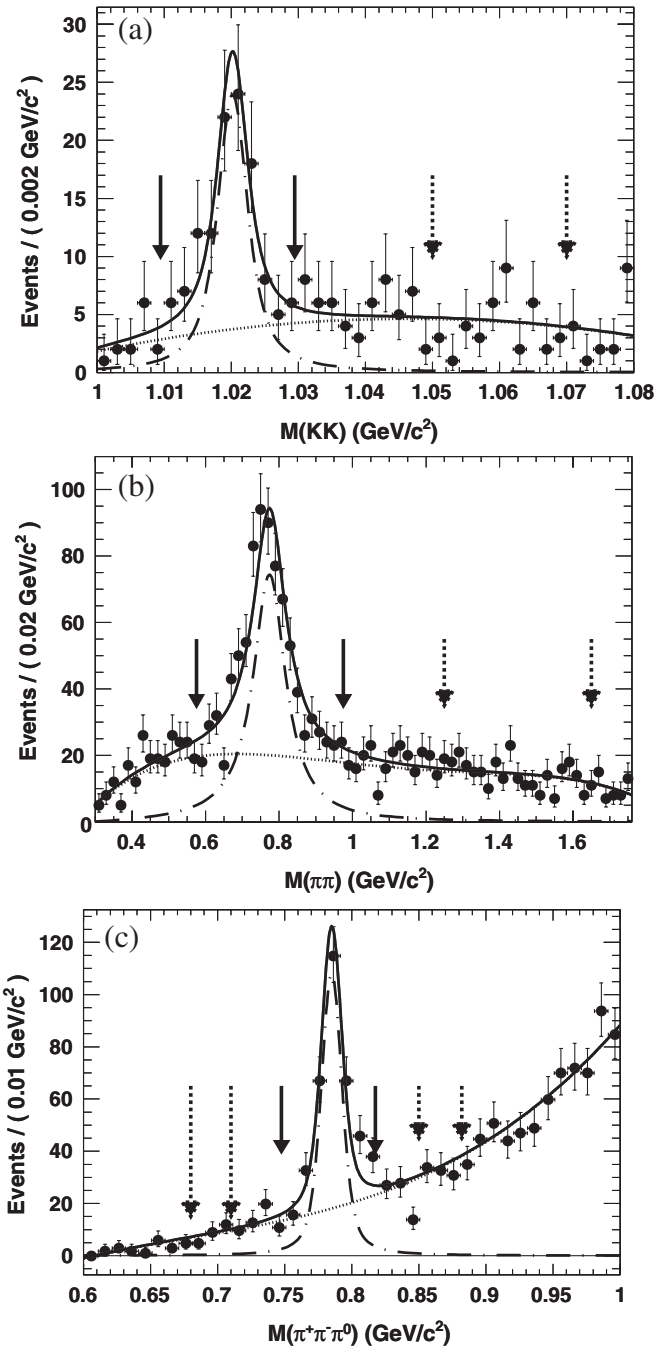

FIG. 1. Invariant mass distributions of (a) K^+K^-, (b) $\pi^+\pi^-$, and (c) $\pi^+\pi^-\pi^0$. Dots with error bars are data; dashed lines are signal shapes; and dotted lines are the polynomial background contributions. The signal regions and sideband regions are indicated with the solid and dashed arrows, respectively.

s-dependent Breit-Wigner function for signal and a polynomial for background. Events with $|M_{K^+K^-} - M_\phi| \leq 0.01$ GeV/c^2, $|M_{\pi^+\pi^-} - M_\rho| \leq 0.2$ GeV/c^2, and $|M_{\pi^+\pi^-\pi^0} - M_\omega| \leq 0.035$ GeV/c^2 are taken as ϕ, ρ^0, and ω candidates, respectively. Here M_ϕ, M_ρ, and M_ω are the nominal masses of these vector mesons. The

sideband regions are defined as $1.05 \leq M_{K^+K^-} \leq 1.07\,\mathrm{GeV}/c^2$, $1.25 \leq M_{\pi^+\pi^-} \leq 1.65\,\mathrm{GeV}/c^2$, and ($0.68 \leq M_{\pi^+\pi^-\pi^0} \leq 0.71\ \mathrm{GeV}/c^2$ and $0.85 \leq M_{\pi^+\pi^-\pi^0} \leq 0.88\ \mathrm{GeV}/c^2$) for the ϕ, ρ^0, and ω, respectively.

After applying the above criteria, there are still several peaking backgrounds in the χ_{cJ} mass regions from χ_{cJ} decays into non-γV modes with the same final states. From MC studies, the shapes of these backgrounds are found to be similar to those of the vector-meson sideband background events. The invariant mass distributions of $\gamma_h V$, where $V = \phi$, ρ^0, ω, respectively, are shown in Figs. 2(a)–2(c). There are clear χ_{c1} signals in all decay modes, while χ_{c0} and χ_{c2} signals are not evident. In order to extract the signal yields from the mass spectra, we first obtain signal shapes for each $\chi_{cJ} \to \gamma V$ mode (9 decay modes in total) using MC simulations. Each of the distributions in Fig. 2 is fitted with a background shape composed of the vector-meson mass sideband distribution plus a 2nd order polynomial function and three χ_{cJ} resonances as the signal shapes. Parameters of the polynomial function and the normalization for each of the χ_{cJ} resonances are allowed to float in the fit. Their systematic errors are listed in Table II, and will be discussed in more detail in the next section. The fitted yields are summarized in Table III. $\chi_{c1} \to \gamma\rho$ and $\gamma\omega$ are observed with a statistical significance larger than 10σ, and the significance for $\chi_{c1} \to \gamma\phi$ is 6.4σ. Here, the significance is determined from $\sqrt{-2\log(\mathcal{L}_0/\mathcal{L}_{\max})}$, where $\mathcal{L}_{\max}$ is the maximum likelihood value, and $\mathcal{L}_0$ is the likelihood for a fit with the signal contribution set to zero. Branching fractions are calculated after considering the signal efficiency, as listed in Table III, and the upper limits at the 90% C.L on the branching factions of χ_{c0} and χ_{c2} decays are estimated by a Bayesian method [17]. The effects of both the statistical and systematic uncertainties to the upper limits are taken into account. All results are listed in Table III.

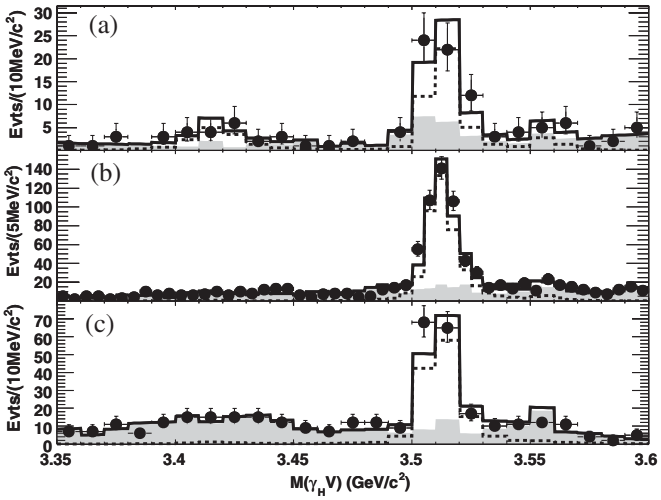

FIG. 2. Invariant mass distributions of (a) $\gamma\phi$, (b) $\gamma\rho^0$, and (c) $\gamma\omega$. Dots with error bars are data; histograms are the best fit; dashed histograms are signal shapes; and the gray-shaded histograms are the sum of the sideband background and the background polynomial.

IV. ESTIMATION OF SYSTEMATIC UNCERTAINTIES

Table II shows the summary of all sources of systematic uncertainties. Many systematic uncertainties are determined using clean, high statistics control samples that allow results from MC simulation to be compared with those from data.

A. Photon efficiency

The photon detection efficiency and its uncertainty are studied by three different methods.

The missing photon method uses a sample of $\psi' \to \pi^+\pi^- J/\psi$, $J/\psi \to \rho^0\pi^0$ events. Using events with four charged tracks, identified as pions, plus a good photon, the missing momentum is determined and used to predict the direction and energy of the missing photon. To remove background, the invariant mass of the good photon and the missing momentum must be consistent with that of the π^0, and the invariant mass of the charged tracks from the J/ψ decay must be consistent with that of the ρ. The photon detection efficiency is then the fraction of actual photons matched in direction to the predicted photon. On average, the efficiency difference between data and Monte Carlo simulation is less than 1%.

The missing π^0 method uses a sample of $\psi' \to \pi^0\pi^0 J/\psi$, $J/\psi \to l^+l^-$ events, in a similar way to the first method. Events with two charged tracks and at least two photons are required. The invariant mass of the charged tracks must be consistent with the mass of the J/ψ, and the sum of the momenta of the two photons must be greater than 300 MeV/c. Since the two pions are anticorrelated, by requiring a π^0 with momentum larger than 300 MeV/c and using energy-momentum conservation, the energy and direction of the remaining soft π^0 can be predicted. To ensure a clean sample, the invariant mass of the two photons of the selected pion and the mass recoiling against the J/ψ and the selected π^0 must be consistent with that of the π^0. The number of reconstructed π^0s, which match in direction and have two photon invariant mass consistent with the π^0 mass, yields the π^0 detection efficiency. The difference in efficiency between the data and Monte Carlo is less than (1.5 ± 0.5)%; hence the uncertainty of photon detection is less than 1%.

The third method, the π^0 decay angle method [18], utilizes a $J/\psi \to \rho^0\pi^0$ sample. Since the π^0 is from a two-body decay, the momentum of the π^0 is known, and the energy of the lower energy daughter photon is given by $2E_{\mathrm{low}} = \sqrt{P^2_{\pi^0} + M^2_{\pi^0}} - P_{\pi^0}\cos\theta$, where θ is the angle of the photon in the π^0 rest frame with respect to the direction of the π^0 in the J/ψ rest frame. For spin-zero particles like the π^0, the $\cos\theta$ distribution is flat in the range of [0, 1].

TABLE II. Sources of systematic errors (%).

	$\gamma\gamma\phi$	$\gamma\gamma\rho$	$\gamma\gamma\omega$
	χ_{c0}, χ_{c1}, χ_{c2}	χ_{c0}, χ_{c1}, χ_{c2}	χ_{c0}, χ_{c1}, χ_{c2}
Tracking	4.0	4.0	4.0
PID	2.0	2.0	2.0
γ detection	2.0	2.0	4.0
4C-fit	0.7	0.7	···
5C-fit	···	···	3.1
Selection efficiency	2.0	5.0	1.4
BG shape	3.4, 2.6, 3.7	2.4, 2.0, 2.8	3.2, 2.4, 4.1
Binning	2.3, 1.5, 2.4	2.0, 1.0, 2.2	1.0, 0.0, 0.0
Fit range and Sideband regions	2.1, 2.0, 2.5	1.0, 0.9, 1.5	1.0, 0.5, 1.0
Signal shape	0.8	0.8	0.8
No. of ψ' evts	3.8	3.8	3.8
$\mathcal{B}(\psi' \to \gamma\chi_{cJ})$ [14]	3.3, 4.4, 4.0	3.3, 4.4, 4.0	3.3, 4.4, 4.0
V decay [14]	1.0	···	0.8
Total	8.8, 8.8, 9.3	9.5, 9.7, 10.0	9.3, 9.4, 9.8

Hence the $E_{\rm low}$ energy spectrum is intrinsically flat, and the deviation from flatness measures the photon inefficiency as a function of energy. The distribution shows that the efficiency is low at low energy but plateaus starting from 0.1 GeV. A comparison of the photon energy spectrum shape between data and Monte Carlo simulation shows that the average difference is 0.6%. However, this measurement only provides a relative efficiency as a function of photon energy. The absolute efficiency in the plateau region above 0.1 GeV can be determined in data and simulation using high energy electrons from radiative Bhabha events. The electromagnetic showers of electrons and photons in the crystal calorimeter are the same for $E > 0.2$ GeV. The detection efficiency for electrons entering the EMC with $E > 0.2$ GeV is essentially 100% in both data and Monte Carlo simulation, which indicates no significant systematic uncertainty in the simulated efficiency of the EMC.

The above three methods may be affected by photon conversions, mainly in the beryllium beam pipe and inner part of the MDC. A study using samples of $e^+e^- \to \gamma\gamma$, $\gamma \to e^+e^-$ events in which the converted photons are explicitly reconstructed indicates systematic efficiency differences due to material in the interaction region between data and simulation are negligible.

Although each of the above three methods suffers from different shortcomings, such as the resolution and tracking efficiency dependence, they all give consistent results within 1%, showing that the photon efficiency uncertainty is less than 1%.

B. Tracking efficiency

The tracking efficiencies for soft and hard pions are studied with $\psi' \to \pi^+\pi^- J/\psi$, $J/\psi \to l^+l^-(l = e, \mu)$ and $J/\psi \to \rho\pi \to \pi^+\pi^-\pi^0$ event samples, respectively. The transverse momentum for a soft pion is less than 400 MeV/c. The tracking efficiency is calculated with $\epsilon = N_{\rm full}/N_{\rm all}$, where $N_{\rm full}$ indicates the number of events of $\pi^+\pi^- l^+l^-(\pi^+\pi^-\pi^0)$ with all final tracks reconstructed successfully; $N_{\rm all}$ indicates the number of events with one or both charged pion tracks successfully reconstructed in addition to the lepton-pair (π^0) for $\psi' \to \pi^+\pi^- J/\psi$, $J/\psi \to l^+l^-$ ($J/\psi \to \rho\pi \to \pi^+\pi^-\pi^0$). In addition, we require that the direction of the missing momentum should be within the MDC coverage. The missing momentum is calculated using the reconstructed lepton-pair (π^0) and one of the reconstructed pions for the $\psi' \to \pi^+\pi^- J/\psi$, $J/\psi \to l^+l^-$ ($J/\psi \to \rho\pi \to \pi^+\pi^-\pi^0$). A very clean soft pion sample is selected by doing a kinematic fit with the lepton-pair constrained to the J/ψ mass, and background from $J/\psi \to \pi^+\pi^-$ is rejected using muon counter information and is negligible. For the hard pion selected from $J/\psi \to \pi^+\pi^-\pi^0$, the purity of the sample is more that 98%; the small background is from $J/\psi \to K^*K \to K^+K^-\pi^0$ due to misidentification of the kaon as a pion for the reconstructed track. The differences for the soft and hard pion tracking efficiencies between the data and MC are both estimated to be 2%, which is taken as the pion tracking uncertainty.

The kaon tracking efficiency is determined with a sample of $J/\psi \to K^*(892)^0 K_S^0 + c.c \to K_S^0 K^+\pi^- + c.c \to K^+\pi^-\pi^+\pi^- + K^-\pi^+\pi^+\pi^-$ events. The tracking efficiency is calculated in the same way as the pion track efficiency. Here $N_{\rm full}$ is the number of events with a matched kaon track in addition to the three tracks identified as pions, and $N_{\rm all}$ is the number of events with or without a matched kaon and three tracks identified as pions. A clean sample is selected by using a second vertex fit to K_S, and setting stringent mass windows for the K_S and $K^*(892)^0$. The difference in the kaon tracking efficiency is about 2%

between the data and MC, which is taken as the uncertainty of kaon tracking efficiency.

C. Efficiency for particle identification

The efficiencies for pion and kaon PID are obtained with $J/\psi \to \pi^+\pi^-\pi^0$ and $K^+K^-\pi^0$ control samples, respectively. Samples with backgrounds less than 1% are selected by using a narrow π^0 mass window, and requiring one track be identified as a pion (kaon) for $J/\psi \to \pi^+\pi^-\pi^0$ ($K^+K^-\pi^0$) based on the TOF and dE/dx information. The PID efficiency is calculated with $\epsilon(PID) = N_0/(N' + N_0)$, where N_0 (N') denotes the events with the other track identified (not identified) as a pion or kaon. The differences between data and MC for the pion and kaon PID efficiencies are about 2%, and 2% is taken as the systematic error.

D. Selection efficiency

The selection efficiency uncertainties listed in Table II are the systematic errors associated with the selection criteria. Control samples such as $J/\psi \to \rho^0\pi^0$, $J/\psi \to \phi\eta$, and $J/\psi \to \omega\eta$ are used to determine the efficiency difference between data and MC for each selection criterion. The relative efficiency difference between data and MC is defined as

$$\frac{N_D^{\rm with}/N_D^{\rm without} - N_{\rm MC}^{\rm with}/N_{\rm MC}^{\rm without}}{N_D^{\rm with}/N_D^{\rm without}},$$

where $N_D^{\rm with}$ and $N_{\rm MC}^{\rm with}$ are the numbers of data and MC simulation events satisfying the requirement being tested in the control sample, and $N_D^{\rm without}$ and $N_{\rm MC}^{\rm without}$ are the numbers of events without that requirement.

For $\psi' \to \gamma\gamma\phi$, the $J/\psi \to \phi\eta$ control sample is used; the uncertainty for the η veto is determined to be 1.9%, and that for the ϕ selection is 0.5%.

In $\psi' \to \gamma\gamma\rho$, the dominant sources are due to the electron and muon track rejection, the $\cos\theta_{\gamma\gamma}$ requirement, the π^0/η veto, and the selection of the ρ^0 signal, which are determined with the $J/\psi \to \rho^0\pi^0$ sample to be 4.5%, 0.9%, 1.2%, and 1.4%, respectively. For this channel, the uncertainty due to the muon track veto for both the π^+ and π^- (4.5%) is also determined from a study of the very pure $J/\psi \to \rho^0\pi^0$ sample.

In $\psi' \to \gamma\gamma\omega$, the uncertainty due to the background rejection and ω signal selection is determined from the $J/\psi \to \omega\eta$ control sample to be 1.4%.

The total uncertainties due to selection criteria are 2.0%, 5.0%, and 1.4% for $\psi' \to \gamma\gamma\phi$, $\psi' \to \gamma\gamma\rho^0$, and $\psi' \to \gamma\gamma\omega$, respectively.

E. Systematic errors in the fit

Systematic errors in the fit to the $\gamma_h V$ mass distribution originate from the uncertainties in the parametrizations for the signal and background shapes. Uncertainties due to the background shape are obtained by changing the order of the polynomial function in the fit from second order to third order. For the signal shapes, the control sample $\psi' \to \gamma\eta' \to \gamma\gamma\rho$ is used to determine the difference in the $\gamma\rho$ mass resolution between data and MC simulation. Then the MC signal shape for $\psi' \to \gamma\chi_{c1} \to \gamma\gamma\rho^0$ is smeared by convolving it with a Gaussian function corresponding to this resolution difference. Finally a comparison is made between the fit result with the smeared MC shape and that with the unsmeared MC shape; the difference, 0.8%, is taken as the systematic error of the signal shape. The systematic errors for $\psi' \to \gamma\chi_{c1} \to \gamma\gamma\phi$ and $\psi' \to \gamma\chi_{c1} \to \gamma\gamma\omega$ are assumed to be the same.

Since there are not enough signal events for an unbinned fit, different bin sizes (the number of bins changes from 20 to 30 for $\gamma\phi$ and $\gamma\omega$ channels and from 40 to 60 for $\gamma\rho$ channel) are chosen to determine the systematic error associated with the binning. Systematic errors associated with the fitting range, and vector-meson sideband regions are estimated by changing the fitting range from $[3.35, 3.60]$ GeV/c^2 to $[3.30, 3.70]$ GeV/c^2, and the vector-meson sideband regions from $[1.05, 1.07]$ GeV/c^2 to $[1.05, 1.075]$ GeV/c^2 for the $\gamma\gamma\phi$ channel, from $[1.25, 1.65]$ GeVc^2 to $[0.30, 0.40]$ GeV/c^2 and $[1.25, 1.70]$ GeV/c^2 for the $\gamma\gamma\rho^0$ channel, from $[0.68, 0.71]$ GeV/c^2 and $[0.85, 0.88]$ GeV/c^2 to $[0.65, 0.71]$ GeV/c^2 and $[0.85, 0.90]$ GeV/c^2 for the $\gamma\gamma\omega$ channel, respectively.

All errors are summarized in Table II. Finally, the total systematic error varies from 8.8%–10.0% depending on the final state as summarized in Table II.

V. HELICITY AMPLITUDE ANALYSIS

In $\chi_{c1} \to \gamma V$ decays, the final state is a superposition of longitudinal ($\lambda = 0$) and transverse ($\lambda = \pm 1$) polarizations. The angular distribution is

$$\frac{d\Gamma}{\Gamma d\cos\theta} \propto (1 - f_T)\cos^2\Theta + \frac{1}{2} f_T \sin^2\Theta,$$

where $f_T = |A_T|^2/(|A_T|^2 + |A_L|^2)$ is the transverse polarization fraction in the decay and A_L and A_T are the longitudinal and transverse polarization amplitudes, respectively, and Θ is the angle between the vector-meson flight direction in the χ_{c1} rest frame and either the π^+/K^+ direction in the ρ^0/ϕ rest frame or the normal to the ω decay plane in the ω rest frame. By performing a likelihood fit to the angular distributions of the vector-meson decays, we can determine the transverse polarization fraction f_T. We account for the different reconstruction efficiencies for the longitudinally and transversely polarized events using $f_T = f_T^{\rm obs}/(R + (1 - R)f_T^{\rm obs})$, where $f_T^{\rm obs}$ is the fraction of signal from transversely polarized signal events in data, and R is the ratio of the longitudinal and transverse signal efficiencies.

In the likelihood fit, we take events in the χ_{c1} signal region which is defined as $3.49 \le M_{\gamma_h V} \le 3.52$ GeV/c^2.

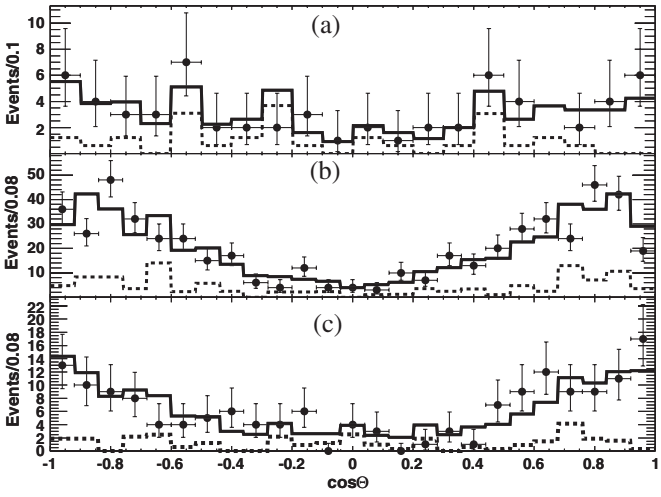

FIG. 3. cosΘ distributions and the fit for (a) $\chi_{c1} \to \gamma\phi$, (b) $\chi_{c1} \to \gamma\rho^0$, and (c) $\chi_{c1} \to \gamma\omega$. Dots with error bars are data; the solid histogram is the fit; and dashed histogram is the sum of the sideband background and the polynomial background.

The signal shapes for the longitudinal and transverse component are obtained from MC simulations. For the background shapes, two sources are considered: one is the vector-meson sideband background, which is normalized according to the number of sideband events in the χ_{c1} signal region; the other background considered is from MC simulated inclusive ψ' decay events (not including signal events) that satisfy the selection criteria and have an invariant mass in the χ_{c1} signal region, which are normalized according to the number of polynomial events used in the χ_{c1} mass fit. The cosΘ distributions are fitted with the combined backgrounds and MC simulated transverse and longitudinal signal shapes. The total signal yield and transverse polarization fraction are floated in the fit. The fitted results are shown in Fig. 3. The values of the fraction of the transverse component are $0.29^{+0.13+0.10}_{-0.12-0.09}$ for $\chi_{c1} \to \gamma\phi$, $0.158 \pm 0.034^{+0.015}_{-0.014}$ for $\chi_{c1} \to \gamma\rho^0$, and $0.247^{+0.090+0.044}_{-0.087-0.026}$ for $\chi_{c1} \to \gamma\omega$, where the first errors are statistical from the fit and the second ones are the systematic errors.

Since f_T is a ratio, many systematic errors cancel out, and only the effects due to binning of the cosΘ distributions and the parametrization of the background shape (estimated by assuming the backgrounds (except for the vector-meson sideband background) contribute entirely to either the longitudinal or the transverse component) are considered here. The uncertainties of the binning of cosΘ are estimated to be $+15.4 - 19.2\%$, $+1.9 - 0.6\%$, and $+2.5 - 0.5\%$, and the parametrization of the background, which is the dominant systematic error, is estimated to be $+28.5 - 23.1\%$, $+9.3 - 9.2\%$, and $+17.6 - 10.5\%$ for $\chi_{c1} \to \gamma\phi$, $\chi_{c1} \to \gamma\rho^0$, and $\chi_{c1} \to \gamma\omega$, respectively. In order to compare with CLEO-c's results, CLEO-c's $A_{\pm}/A_0$ have been used to determine f_T as: $0.072^{+0.041+0.002}_{-0.031-0.019}$ for $\chi_{c1} \to \gamma\rho$, and $0.32^{+0.17+0.05}_{-0.11-0.11}$ for $\chi_{c1} \to \gamma\omega$. The results are consistent within 2σ.

VI. FINAL RESULTS AND DISCUSSION

In summary, we present the measurements of radiative decays of χ_{cJ} to light vector mesons. We find $\mathcal{B}(\chi_{c1} \to \gamma\rho^0) = (228 \pm 13 \pm 16) \times 10^{-6}$ and $\mathcal{B}(\chi_{c1} \to \gamma\omega) = (69.7 \pm 7.2 \pm 5.6) \times 10^{-6}$, which agree with the results from the CLEO experiment [6]. We observe $\chi_{c1} \to \gamma\phi$ for the first time, and find $\mathcal{B}(\chi_{c1} \to \gamma\phi) = (25.8 \pm 5.2 \pm 2.0) \times 10^{-6}$. Upper limits at the 90% confidence level on the branching fractions for χ_{c0} and χ_{c2} decays into these final states are determined. The final results are listed in Table III. The theoretical predictions for $\mathcal{B}(\chi_{c1} \to \gamma V)$ including the hadronic loop contribution in pQCD calculation [7] are consistent with our measurements within errors. In addition, the fraction of the transverse polarization component of the vector meson in $\chi_{c1} \to \gamma V$ decay is studied. Our measurements of the polarization of the vector mesons indicate that the longitudinal component is dominant in $\chi_{c1} \to \gamma V$ decay, as expected for an axial-vector particle radiative decaying into a vector (ϕ, ρ^0, and ω) in the framework of the vector dominance model taking into account the Landau-Yang theorem [19,20]. This observation may aid future development on the QCD calculation of the partial waves in the $\chi_{c1} \to \gamma V$ decay.

TABLE III. Results on $\chi_{cJ} \to \gamma V$. The upper limits are set at the 90% C.L.

Decay mode	No. of evts.	Eff. (%)	Syst. err.(%)	Br. (10^{-6})	Stat. sign.
$\chi_{c0} \to \gamma\phi$	15.0 ± 6.6	32.4	8.8	<16.2	
$\chi_{c1} \to \gamma\phi$	42.6 ± 8.6	34.6	8.8	$25.8 \pm 5.2 \pm 2.3$	6σ
$\chi_{c2} \to \gamma\phi$	4.6 ± 4.9	32.6	9.3	<8.1	
$\chi_{c0} \to \gamma\rho^0$	6 ± 12	22.6	8.1	<10.5	
$\chi_{c1} \to \gamma\rho^0$	432 ± 25	19.4	8.3	$228 \pm 13 \pm 22$	$>10\sigma$
$\chi_{c2} \to \gamma\rho^0$	13 ± 11	15.7	8.7	<20.8	
$\chi_{c0} \to \gamma\omega$	5 ± 11	18.6	9.3	<12.9	
$\chi_{c1} \to \gamma\omega$	136 ± 14	22.7	9.4	$69.7 \pm 7.2 \pm 6.6$	$>10\sigma$
$\chi_{c2} \to \gamma\omega$	1 ± 6	19.2	9.8	<6.1	

ACKNOWLEDGMENTS

The BESIII collaboration thanks the staff of BEPCII and the computing center for their hard efforts. This work is supported in part by the Ministry of Science and Technology of China under Contract No. 2009CB825200; National Natural Science Foundation of China (NSFC) under Contracts Nos. 10625524, 10821063, 10825524, 10835001, 10935007; the Chinese Academy of Sciences (CAS) Large-Scale Scientific Facility Program; CAS under Contracts Nos. KJCX2-YW-N29, KJCX2-YW-N45; 100 Talents Program of CAS; Istituto Nazionale di Fisica Nucleare, Italy; Russian Foundation for Basic Research under Contracts Nos. 08-02-92221, 08-02-92200-NSFC-a; Siberian Branch of Russian Academy of Science, joint project No. 32 with CAS; U. S. Department of Energy under Contract Nos. DE-FG02-04ER41291, DE-FG02-91ER40682, DE-FG02-94ER40823; University of Groningen (RuG) and the Helmholtzzentrum fuer Schwerionenforschung GmbH (GSI), Darmstadt; WCU Program of National Research Foundation of Korea under Contract No. R32-2008-000-10155-0

[1] S. Dulat and B. S. Zou, Eur. Phys. J. A **26**, 125 (2005).
[2] Y. J. Gao, Y. J. Zhang, and K. T. Chao, Chin. Phys. Lett. **23**, 2376 (2006).
[3] Y. J. Gao, Y. J. Zhang, and K. T. Chao, arXiv:hep-ph/0701009.
[4] F. Close *et al.*, Phys. Rev. D **67**, 074031 (2003).
[5] C. Amsler and F. E. Close, Phys. Rev. D **53**, 295 (1996).
[6] J. V. Bennett *et al.* (CLEO Collaboration), Phys. Rev. Lett. **101**, 151801 (2008).
[7] D. Y. Chen, Y. B. Dong, and X. Liu, Eur. Phys. J. C **70**, 177 (2010).
[8] M. Ablikim *et al.*, Nucl. Instrum. Methods Phys. Res., Sect. A **614**, 345 (2010).
[9] J. Z. Bai *et al.* (BES Collaboration), Nucl. Instrum. Methods Phys. Res., Sect. A **344**, 319 (1994); **458**, 627 (2001).
[10] Special issue on Physics at BES-III, edited by K. T. Chao and Y. F. Wang, [Int. J. Mod. Phys. A **24**, Supp. (2009) http://www.worldscinet.com/ijmpa/24/24supp01/S0217751X0924supp01.html]
[11] Z. Y. Deng *et al.*, High Energy Physics & Nuclear Physics **30**, 371 (2006).
[12] S. Jadach, B. F. L. Ward, and Z. Was, Comput. Phys. Commun. **130**, 260 (2000); Phys. Rev. D **63**, 113009 (2001).
[13] R. G. Ping *et al.*, High Energy Physics & Nuclear Physics **32**, 599 (2008).
[14] K. Nakamura *et al.* (Particle Data Group), J. Phys. G **37**, 075021 (2010).
[15] J. C. Chen, G. S. Huang, X. R. Qi, D. H. Zhang, and Y. S. Zhu, Phys. Rev. D **62**, 034003 (2000).
[16] W. D Li, H. M Liu *et al.*, in *Proceedings of CHEP06, Mumbai, India, 2006* edited by Sunanda Banerjee (Tata Institute of Fundamental Research , Mumbai, 2006).
[17] ZHU Yong-sheng, Chinese Phys. C **32**, 363 (2008).
[18] S. M. Li *et al.*, High Energy Phys. Nucl. Phys. **28**, 859 (2004).
[19] D. V. Amelin *et al.* (VES Collaboration), Z. Phys. C **66**, 71 (1995).
[20] C. N. Yang, Phys. Rev. **77**, 242 (1950).